JOURNAL OF MATERIALS SCIENCE 22 (1987) 1265–1270

Growth and electrical properties of Zn_3P_2 single crystals and polycrystalline ingots

D. DECROIX, V. MUÑOZ*, A CHEVY
Physique des Milieux Condenses U.A. 782, Université Pierre et Marie Curie, 4 Pl. Jussieu, 75230 Paris Cedex 05, France

A method to grow tetragonal α-Zn_3P_2 single crystals from commercially available powder is reported. Thermal and growth duration conditions to increase crystal quality are given. The applicability of the Klosse–Ullersma model is discussed in this case, and optimized reactor dimensions are given. To grow polycrystalline ingots in a standard two-zone furnace from synthesis of elements, we propose a method which allows one to obtain single compact polycrystals with as-grown resistivities comparable to the best values reported for Zn_3P_2. Finally the growth of Zn_3P_2 and silver-doped Zn_3P_2 in the proportions 0.01 to 0.1 at% Ag per atom of zinc are for the first time reported. Crystallographic and electrical properties are also studied.

1. Introduction

Zinc phosphide has been recognized to be a promising photovoltaic material and efforts have been made to improve the crystal growth of this semiconductor. Examination of the Zn-P phase diagram [1, 2] shows that three parameters will limit the use of growth methods from the melt: (i) the temperature of fusion ($\approx 1193°$ C) is relatively high, (ii) the vapour pressure at melting is above 3 bar (3×10^5 Pa) according to the curve published by Greenberg *et al.* [3], (iii) a solid–solid phase transition occurs at 880° C. These reasons can explain why up to now, to our knowledge, only one paper deals with the growth of Zn_3P_2 from the liquid phase. The liquid-encapsulated Czochralski method was used by Moller *et al.* [4] under 30 bar (3 MPa) of argon.

Zinc phosphide sublimes with congruent decomposition. Species in the gas phase are zinc, P_4 and P_2. This equilibrium was studied by Schoonmaker *et al.* [5] and the equilibrium constant established. The properties discussed above explain why growth methods for the vapour phase are most frequently reported in the literature. Small samples have been produced by simple sublimation [6–8]. Large Zn_3P_2 crystals have also been grown in the vapour phase by a Bridgman method [9, 10] and by a perforated capsule technique [11]. Iodine transport has also been tried [9].

This review of literature shows that, in general, Zn_3P_2 is grown from the synthesis of constituant elements in stoichiometric proportions and a specific arrangement is used to obtain good-quality crystals of Zn_3P_2. On the other hand, as-grown crystals have a relatively high resistivity and have to undergo further treatment to bring it down to values compatible with device requirements.

The applicability of Zn_3P_2 for photovoltaic devices being limited by the cost of manufacturing processing and material production, we have studied its growth in a standard two-zone furnace, establishing the conditions for better results, and using low-cost material as source (commercial powder of Zn_3P_2). Growth parameters are improved and experimental results are interpreted in terms of the Klosse–Ullersma model [12]. In those exploratory experiments only small samples were grown with dimensions below photovoltaic cells requirements. We next developed a simple method to make large compact polycrystalline boules. On the other hand, the early elaborated single crystals presented erratic and too resistive properties. Doping processes were achieved to get better control of the electrical properties of zinc phosphide.

2. Growth experiments

2.1. Experimental procedure

From the review presented in the introduction, sublimation seems to be the most suitable method to grow zinc phosphide crystals.

All our experiments of growth by physical vapour transport (PVT) were performed in a classical two-zone furnace, the temperature profile of which is shown in Fig. 1. Quartz ampoules were carbon-coated by cracking methane at 1000° C to prevent the chemical reaction of zinc with silica. Ampoules containing the source material were sealed off under a vacuum better than 10^{-5} mbar (1 Pa). The charge mass was about 15 g. In earlier growth runs, commercially available Zn_3P_2 powder was used (Prolabo Lab, Paris).

A first series of growth experiments was performed to establish the best thermal conditions (i.e. conditons to obtain the largest single crystals) and to study the influence of growth parameters upon mass transport rate. In ampoules with 2 cm inner diameter and 20 cm length, well-developed samples were obtained with source temperature $T_1 = 825°$ C and deposit temperature $T_2 = 610°$ C. Decreasing the temperature gradient $\Delta T = T_1 - T_2$ led to a decrease of the

*On leave from the Departamento de Electricidad y Magnetismo, Facultat de Fisiques, Valencia, Spain.

0022–2461/87 $03.00 + .12

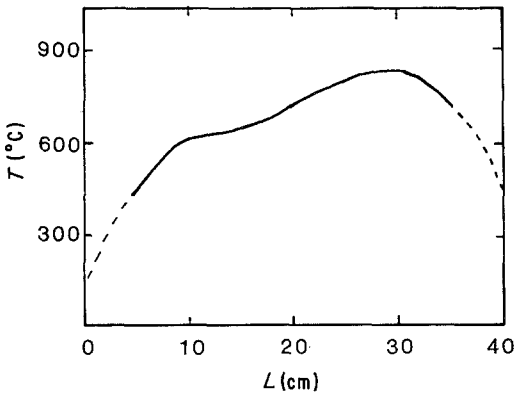

Figure 1 Temperature gradient of the two-zone furnace used for the growth of single crystals and polycrystalline samples.

quantity of transported material and crystals were of poorer quality.

2.2. Synthesis of Zn_3P_2 from pure elements

In order to have a better control of electrical properties, Zn_3P_2 was synthesized in an horizontal single-zone furnace by reaction of stoichiometric proportions of high purity zinc (> 5.8 N) and red phosphorus (> 6 N). When required, doping agents phosphorus or silver were added to the charge. The ampoule was loaded into the furnace and a third part of the tube's length was left out of the furnace to avoid the risk of explosion when the temperature was raised. This process was carried out at a rate of $50^\circ C\,h^{-1}$ up to 450° C. Thus the phosphorus goes to the cooler zone and is partly converted into the white form which is more volatile and hence more suitable for reaction by vapour-phase synthesis. Moreover, white phosphorus makes it possible to raise the temperature without any risk of explosion. Next the tube was completely introduced into the furnace (the cooler zone of the ampoule at the end of the furnace). This configuration was maintained for 16 h. Then, the temperature of the hotter part was raised at the same rate up to 850° C and remained there for 16 h. By that time the reaction was completed and the resulting product was a small quantity of needle-like crystals of Zn_3P_2 and a coarse-grained polycrystalline mass on the walls of the ampoule.

2.3. Growth of polycrystalline boules

Crystal growth experiments were done in the same standard two-zone horizontal furnace, the temperature gradient of which is shown in Fig. 1. Carbon-coated silica tubes 20 cm in length, inner diameter 2 cm were used. The crucible was loaded with the source material, obtained as described above, and sealed under 6×10^{-6} mbar (0.6 Pa) vacuum, then was placed in the furnace. In a first stage (24 h) the growth region was heated to 800° C and the source was kept at 600° C, in order to remove parasitic nuclei from the growth zone. After inverse transport, the growth itself was carried out in two stages. In the first one, the source was kept at 800° C for 24 h and the cooler or growth zone at 750° C, to allow a slight nucleation process. In the second stage the temperature of the cooler zone was decreased to 700° C while the hotter zone was kept at 800° C for 6 days. The result of all these experiments was a compact polycrystalline ingot 3 to 4 cm long, and 2 cm in diameter in the growth zone.

3. Transport rate

3.1. Variation of transport rate with growth duration

The transport rate is know to be dependent upon the duration of experiment. To measure the evolution of the transport rate for this material and to optimize it, the experimental procedure proposed by Jeffes and Marples [13] was used. The arrangement is presented in Fig. 2. The ampoule was 2 cm i.d. and 20 cm long. The extension rod was 35 cm in length. The results of this study are shown in Fig. 3.

In a first stage (for the initial 35 h), the apparent growth rate (weight to restore the balance equilibrium over time) is about $7.7\,mg\,h^{-1}$ which corresponds to an actual growth rate of about $32\,mg\,h^{-1}$ (i.e. taking into account the position of transported mass). This step can be interpreted as a nucleation period during which the crystallization zone is covered by thin

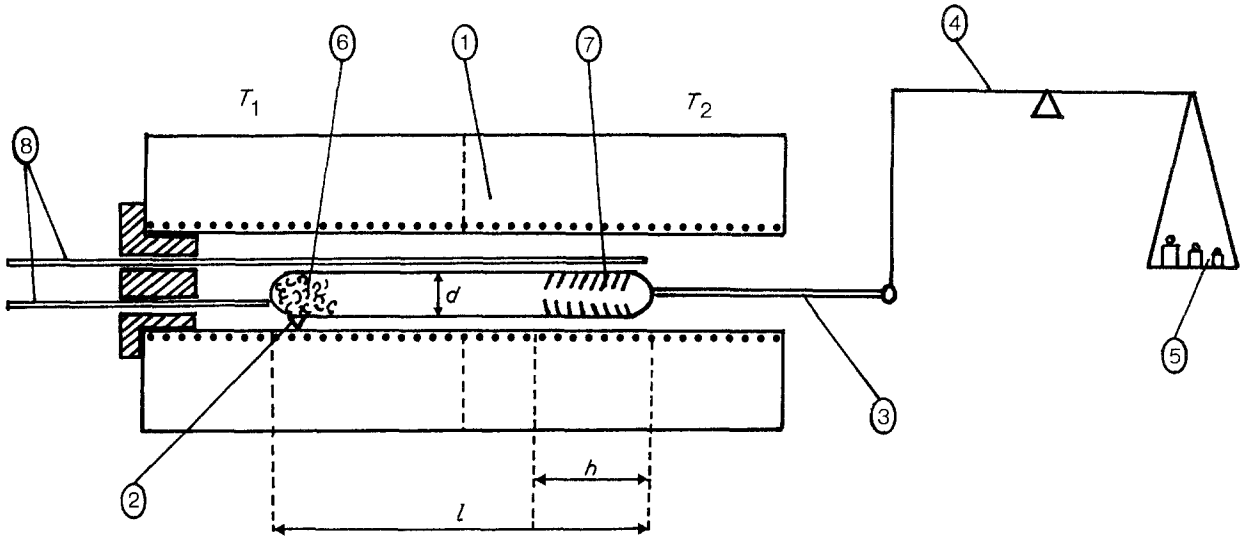

Figure 2 Design of the apparatus for *in situ* measurement of the apparent growth rate [11]. (1) Two-zone furnace, (2) silica pivot, (3) silica extension rod, (4) scale, (5) apparent mass, (6) powder source, (7) crystals (8) thermocouples.

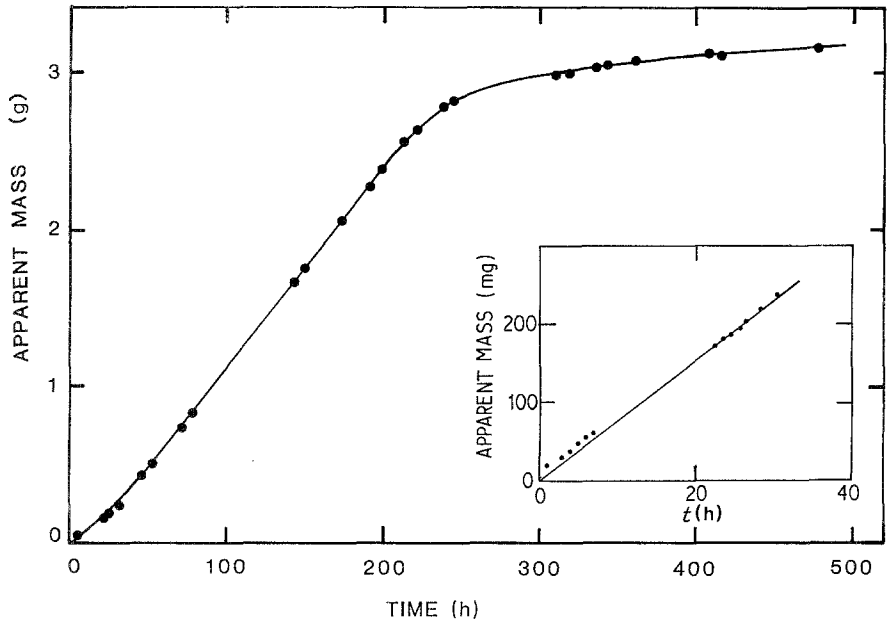

Figure 3 Apparent mass of Zn_3P_2 deposit against time. Saturation of the mass transport occurs after approximately 220 h. (Insert, on an enlarged scale, the beginning of the growth run.)

polycrystalline layers. In the second part of the curve, a constant apparent growth speed of 12.9 mg h^{-1}, which corresponds to an actual rate of about 53 mg h^{-1} appears; this agrees well with the results of experiments performed in a "normal" way (see next section). During this stage, which lasts from 40 to 200 h approximately, thick, coarse-grained polycrystalline layers develop and upon these, individual large crystals grow.

After 225 h, the growth rate apparently saturates and tends to a constant value of about 3 mg h^{-1} for $t = 480$ h. This saturation cannot be explained by the exhaustion of the source because a large excess of material remains in the crucible after the run. Although a displacement of the centre of gravity of our system cannot be totally excluded, a more likely explanation can be found either in a saturation of the growth sites or in a reduction of the mass transport by decrease of the effective inner diameter of the ampoule. Another possibility would be an increase of the residual pressure of non-reacting species [9].

3.2. Application of the Klosse–Ullersma model

It is usually assumed that diffusion and/or convection are responsible for mass transport in vapour-growth processes and several models of transport by diffusion have been developed. It is more difficult to take into account convection in a quantitative analytic form. Klosse and Ullersma (KU) [12] represent the ratio K of the contribution of the flux of convection J_C to the contribution of the flux of diffusion J_D as

$$\frac{J_C}{J_D} = \frac{1}{A(S_c G_r)^{-2} + B}$$

where S_c and G_r are the Schmidt and Grashof numbers. A and B are dimensionless quantities which can be evaluated as a function of the aspect factor l/d (l is the length of the reactor, d its diameter).

The applicability of this model has been tested by a set of growth experiments with ampoules between 10 and 20 cm long and 0.6 to 4 cm inner diameter, the temperatures of growth and source zones being respectively 610 and 825° C. The growth time was 167 h. Typical experimental results are shown in Figs 4 and 5. In Fig. 4 the total flux ($J_T = J_D + J_C$) is plotted as a function of diameter for a given length of ampoule. In Fig. 5 the total flux is plotted as a function of the length of the ampoule.

A simultaneous fit of these experimental curves with the KU model gives a value for the product of Schmidt and Grashof's numbers

$$\frac{S_c G_r}{d^3} = 1.75 \times 10^5 \text{cm}^{-3}$$

and taking into account their definition it is easily proven that

$$\frac{1}{\eta D}\frac{\partial \varrho}{\partial T} = 0.828 \text{cm}^{-4}\text{sec}^2\text{K}^{-1}$$

where η, D, ϱ and T are the viscosity, diffusion coefficient, density and temperature, respectively. The lack of η, D, ϱ values for the $Zn–P_4–P_2$ system does not allow us to separate the individual values at the

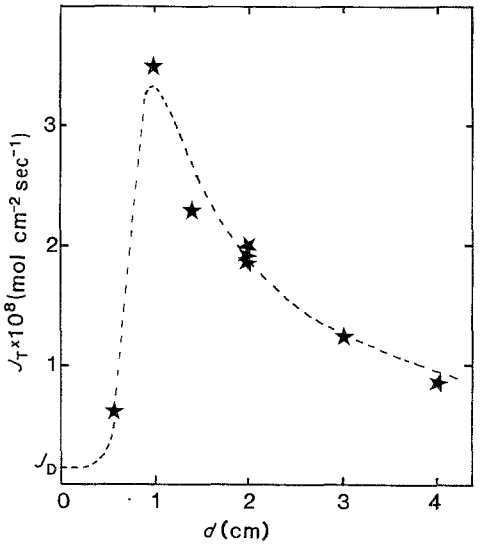

Figure 4 Total flux of transported Zn_3P_2 against diameter of ampoule. Ampoule length: 20 cm, growth time: 167 h. (★) Experimental points, (---) fit with the Klosse–Ullersma model.

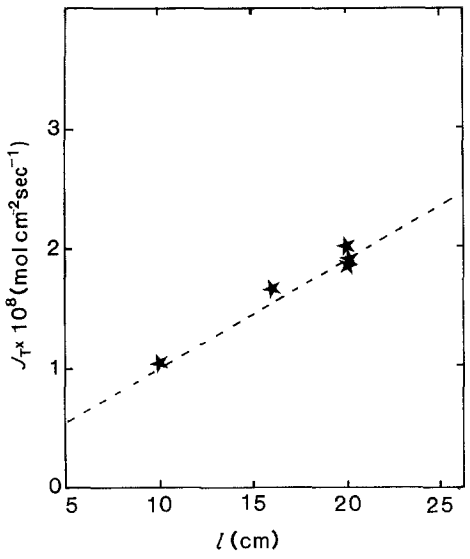

Figure 5 Total flux against length of ampoule. Ampoule diameter: 2 cm, growth time: 167 h. (★) Experimental points, (– – –) fit with the Klosse–Ullersma model.

present time. The calculated flux of diffusion will be

$$J_D = 1.45 \times 10^{-9} \text{mol cm}^{-2}\text{sec}^{-1}$$

This good fit of the KU model with our results permits a semiquantitative evaluating of the kinetics of transport by sublimation in Zn_3P_2. In other words this means that: (i) the aspect factor l/d plays a very important role in determining the total flux (i.e. the quantity of transported material), (ii) there is a geometrical dimension of reactor for which the total flux is maximum and (iii) thermal convection is preponderant during transport by sublimation of Zn_3P_2.

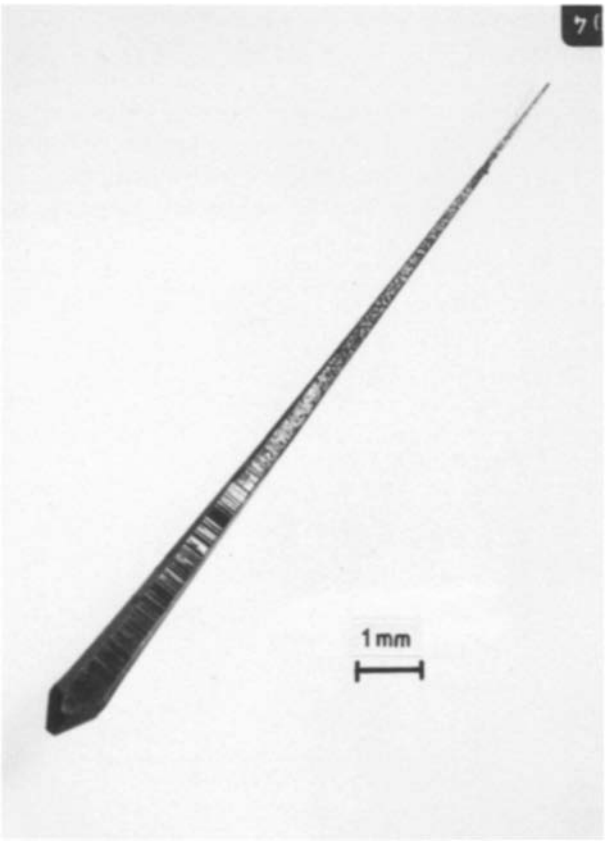

Figure 6 Photograph of a [0 2 1] Zn_3P_2 needle. Growth striae are clearly visible.

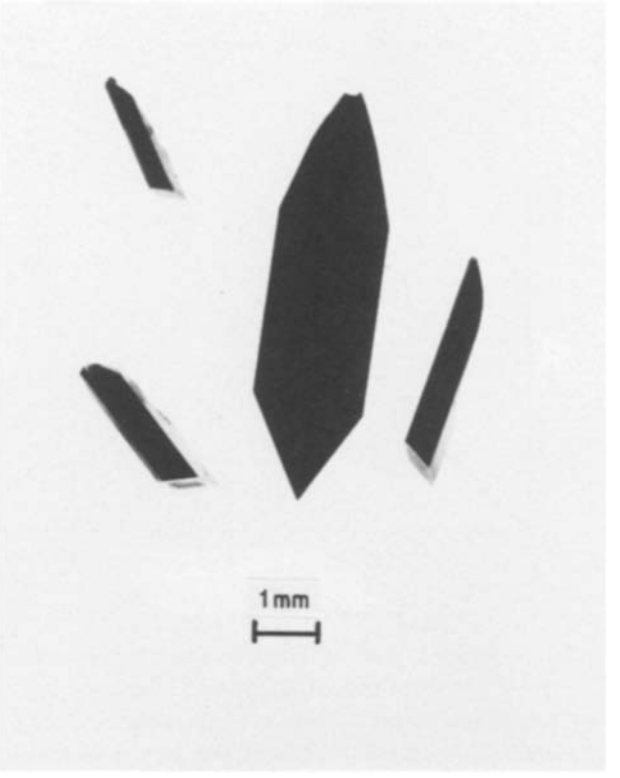

Figure 7 (1 0 1) platelet and [1 0 0] prisms.

3.3. Crystallographic characterization

3.3.1. Single-crystals habits

Zinc phosphide is quadratic with a $P4_2/n\,m\,c$ space group. Lattice parameters have been reported to be $a = 0.8097$ nm and $c = 1.145$ nm. Our X-ray measurements agree with those values. Crystal orientation was done on samples grown from commercial powder, by the rotating crystal method. Dimensions of crystals were in the millimetre range. As reported earlier [6], Zn_3P_2 crystals exhibit several habits such as prisms, needles or platelets. Fig. 6 shows a [0 2 1] needle which develops along the diagonal of the elementary cube. On its faces, growth striae are visible as already reported by Zdanowicz *et al.* [7]. In the centre of Fig. 7 a thin (1 0 1) platelet is visible. The three prisms surrounding the platelet develop in the [1 0 0] direction. The lateral planes are (0 1 1), (0 $\bar{1}$ $\bar{1}$), (0 $\bar{1}$ 1) (0 1 $\bar{1}$) and a small face is recognized to be a (0 0 1) plane (see Fig. 8). It

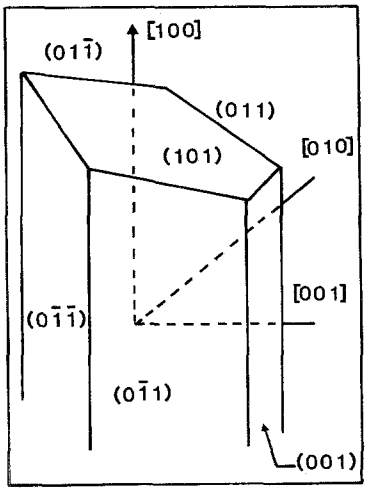

Figure 8 Indexation of faces of a [1 0 0] prism.

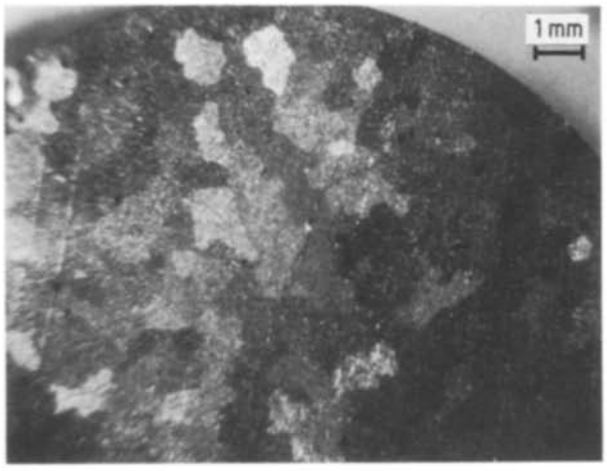

Figure 9 Non-etched polycrystalline Zn_3P_2 sample. Grain sizes are in the 1 to 3 mm range

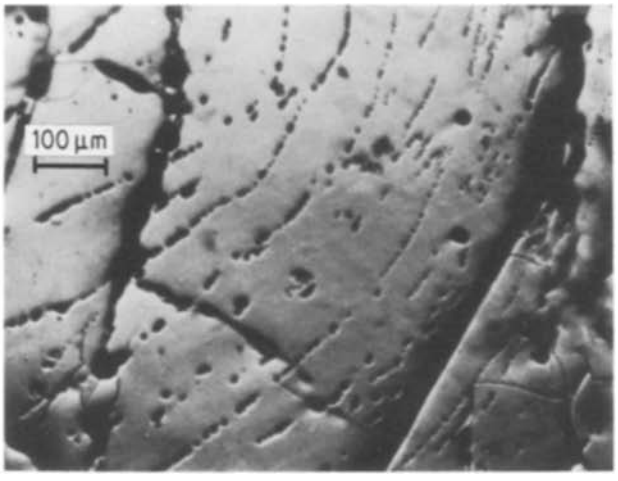

Figure 10 Grain boundaries and etch pit lines revealed by chemical etching polycrystalline samples.

terminates by a (1 0 1) face that has the same orientation as the lamellae.

3.3.2. Polycrystalline ingots

Polycrystalline boules were obtained by the method described in Section 2.3. Mechanically cut and polished wafers were chemically etched in relatively high concentration (3%) bromine–methanol solution for about 15 min, then rinsed out with methanol. When dried, wafers were observed under a microscope.

In Fig. 9, we can observe on an unetched sample the grained structure of the ingot. The grain sizes are in the range of 1 to 3 mm. In Fig. 10 the etch pattern shows grain boundaries and etch pit lines which point to non-basal dislocations. Concentric dislocations lines run across boundary layers. In this picture and when etch pits are randomly distributed, the dislocations density is about 10^4 to $10^5\,cm^{-2}$.

4. Electrical characterization

Electrical properties published in the literature exhibit a wide spread of values [4, 11, 14–19] which is expected if they mostly depend on growth conditions. Resistivity values extend from 10 to $10^6\,\Omega cm$, Hall mobilities of the holes from 10 to $50\,cm^2\,V^{-1}\,sec^{-1}$ and carrier concentrations from 10^{12} to $10^{16}\,cm^{-3}$. Catalano and Hall [14] showed that a phosphorus excess in the vapour phase yields rather conductive material whereas a zinc-rich atmosphere gives highly resistive crystals.

Attempts to diffuse silver have been reported [17, 20, 21]. These authors report a definite increase of hole concentration and therefore a decrease of resistivity.

In this paper electrical properties were determined by conductivity and Hall effect measurements at room temperature. The magnetic field was of 1.425 T. Contacts with linear a $I-V$ dependence were obtained with silver paint.

In order to reduce the resistivity, attempts were made to grow doped crystals. In our experiments, doping was achieved during synthesis. A phosphorus concentration of 4 at % and 0.1 to 0.01 at % Ag per atom of zinc were added to the stoichiometric charge of zinc and phosphorus elements.

Some typical results are summarized in Table I. The transport properties of single crystals agree with those published by different authors. Although from our results it is difficult to make a correlation between the resistivity and phosphorus-rich vapour during growth, one can note a slight increase of hole concentration and a decrease of mobility. This effect can be assigned rather to boundary layers effects than to phosphorus doping. The same remark holds for the mobility of silver-doped crystals. Nevertheless, it is clear that doping effects are enhanced: the resistivity is lowered to about $10\,\Omega cm$ and hole concentration raised to $10^{17}\,cm^{-3}$. Material from the growth of sample 946/72 shows a resistivity which is among the lowest reported in the literature.

5. Conclusions

An easy and inexpensive method to grow Zn_3P_2 single crystals by vapour transport has been developed. We have shown that the Klosse–Ullersma model can exactly account for the mass transport kinetics of PVT

TABLE I Electrical properties of as-grown crystals

Sample No.	Nature of material	Resistivity (Ωcm)	Mobility ($cm^2\,V^{-1}\,sec^{-1}$)	Hole concentration (cm^{-3})
735/1	Single crystals from commercial powder	10^5	–	–
739/4	As above	250	50	7×10^{14}
793/25	As above	2100	20	2.5×10^{14}
914/62	Polycrystalline samples growth in phosphorus-rich atmosphere	100	20	6×10^{15}
917/64	As above	2000	3	9×10^{14}
941/70	Polycrystalline samples, 0.1 at % Ag per atom of zinc	30	2	10^{17}
946/72	Polycrystalline samples, 0.01 at % Ag per atom of zinc	4	11	10^{17}

in Zn_3P_2. The aspect factor appears as a dominant parameter and influences the ratio of convective to diffusive flux.

To prepare polycrystalline wafers which can be used as a substrate for photovoltaic devices we suggest a simple method, from the synthesis of elements, which also allows a doping process during the run.

Progress was made in the control of electrical properties and low-resistivity material has been obtained by silver doping.

Acknowledgement

One of us (V.M.) acknowledges the Spanish and French Governments for financial support as a fellowship of the "Plan de Formacion de Personal Investigador".

Reference

1. J. BERAK and Z. PRUCHNIK, *Ann. Soc. Chim. Polon.* **43** (1969) 1141.
2. Ya. A. UGAI, O. Ia. GOUROV, E. P. DOMACHEUSKAIA and L. A. OZEROV, *Neorg. Mater.* **4** (1968) 147.
3. J. H. GREENBERG, V. B. LAZAREV, S. E. KOZLOV and V. J. SHEVCHENKO, *J. Chem. Therm.* **6** (1974) 1005.
4. A. MOLLER, U. ELROD, P. MUNZ, J. HONIGSCHMID, C. CLEMEN and E. BUCHER, *Int. Phys. Conf. Ser.* **43** (1979) 825.
5. R. C. SCHOONMAKER, A. R. VENKITARAMEN and P. K. LEE, *J. Phys. Chem.* **71** (1967) 2676.
6. M. V. STAKELBERG and R. PAULUS, *Z. Phys. Chem.* **B28** (1935) 427.
7. W. ZDANOWICZ, K. KOLC, A. KALINSKA, E. CISOWSKA and A. BURIAN, *J. Cryst. Growth* **31** (1975) 56.
8. E. K. ARUSHANOV, *Prog. Cryst. Growth Charact.* **3** (1981) 211.
9. F. C. WANG, R. H. BUBE, R. S. FIEGELSON and R. K. ROUTE, *J. Cryst. Growth* **55** (1981) 268.
10. V. Ya. SCHEVCHENKO and S. F. MARENKIN, *Neorg. Mater.* **15** (1979) 1106.
11. A. CATALANO, *J. Cryst. Growth* **49** (1980) 681.
12. K. KLOSSE and P. ULLERSMA, *ibid.* **18** (1973) 167.
13. J. H. E. JEFFES and T. N. R. MARPLES, *ibid.* **17** (1972) 46.
14. A. CATALANO and R. B. HALL, *J. Phys. Chem. Solids* **41** (1982) 635.
15. H. U. FINZEL, *J. Cryst. Growth* **50** (1980) 823.
16. E. A. FAGEN, *J. Appl. Phys.* **50** (1979) 6505.
17. F. C. WANG, A. L. FAHRENBRUCH and R. H. BUBE, *J. Elect. Mater.* **11** (1982) 75.
18. J. LAGRENAUDIE, *J. Phys. Radium* **16** (1955) 234.
19. W. ZDANOWICZ and Z. HENKIE, *Bull. Acad. Pol. Sci.* **XII** (1964) 729.
20. T. SUDA, M. KOBAYASHI, A. KUROYANAGI and J. ZURITA, *J. Jpn Appl. Phys.* **21** Suppl. **21**(2) (1982) 63.
21. P. S. NAYAR, *J. Appl. Phys.* **53** (1982) 1069.

Received 16 May
and accepted 23 July 1986